

# Institute for Neural Computation

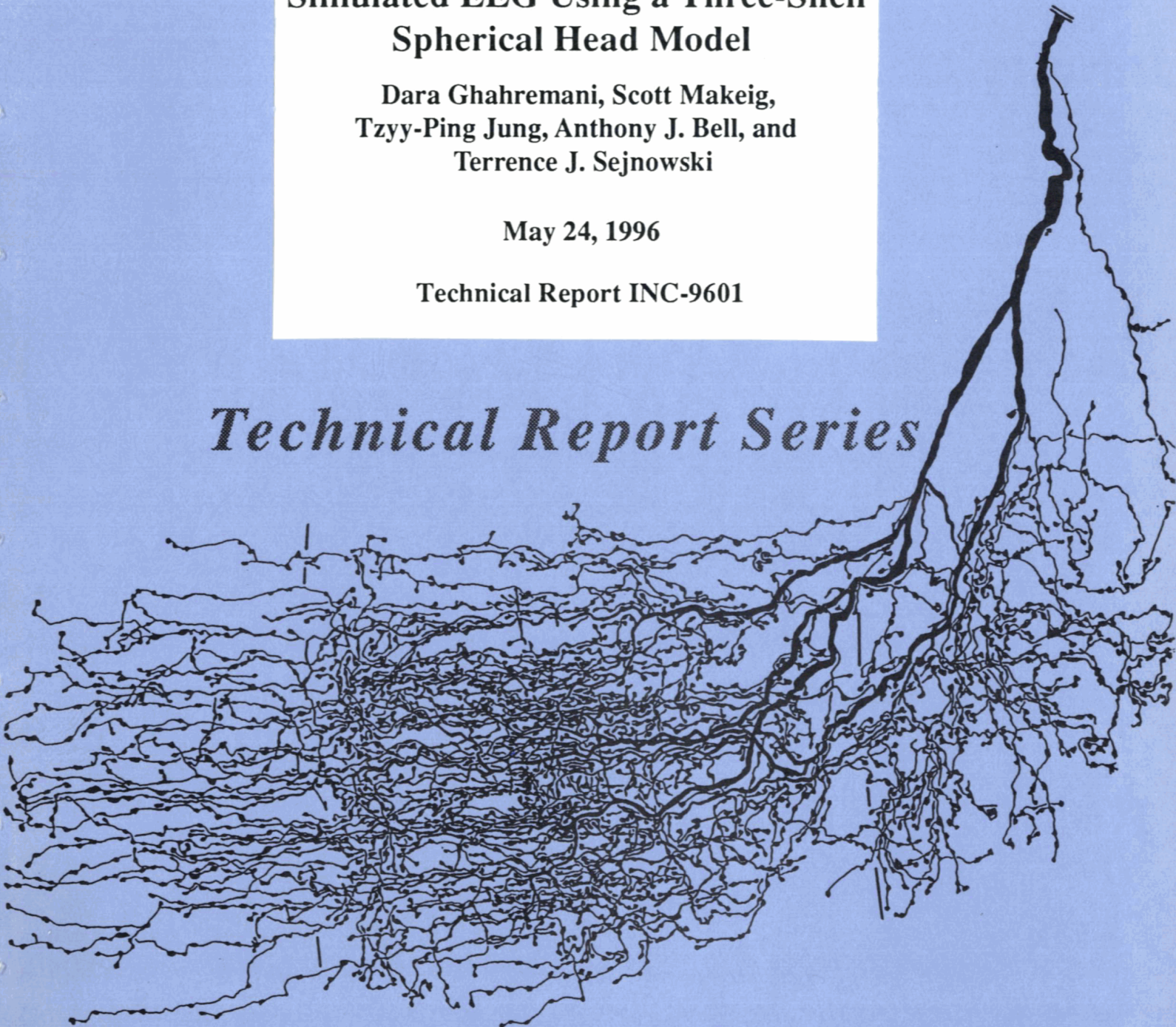
## Independent Component Analysis of Simulated EEG Using a Three-Shell Spherical Head Model

Dara Ghahremani, Scott Makeig,  
Tzyy-Ping Jung, Anthony J. Bell, and  
Terrence J. Sejnowski

May 24, 1996

Technical Report INC-9601

*Technical Report Series*



# Independent Component Analysis of Simulated EEG Using a Three-Shell Spherical Head Model

Dara Ghahremani, Scott Makeig,  
Tzyy-Ping Jung, Anthony J. Bell, and  
Terrence J. Sejnowski

May 24, 1996

Technical Report INC-9601

*Institute for Neural Computation  
University of California, San Diego  
9500 Gilman Drive, DEPT 0523  
La Jolla, CA 92093-0523*

Dara Ghahremani, Tzyy-Ping Jung, Anthony J. Bell, and Terrence J. Sejnowski are with the Computational Neurobiology Lab, a Howard Hughes Medical Institute laboratory, at The Salk Institute for Biological Studies. Scott Makeig is with the Naval Health Research Center and the Department of Neuroscience at the University of California, San Diego. Terrence J. Sejnowski is also with the Institute for Neural Computation at the University of California, San Diego.

This research was supported in part by grants from the Navy Medical Research and Development Command and the Office of Naval Research, Department of the Navy under work unit ONR.Reimb-6429 and the Howard Hughes Medical Institute. The views expressed in this article are those of the authors and do not reflect the official policy or position of the Department of the Navy, Department of Defense, or the U.S. Government. The authors wish to thank Anders Dale for supplying the head model parameters.

Correspondence concerning this article may be addressed to: Scott Makeig, Naval Health Research Center, P. O. Box 85122, San Diego, CA 92186-5122 (email: scott@salk.edu).

Copyright © 1996 by Dara Ghahremani, Scott Makeig, Tzyy-Ping Jung, Anthony J. Bell and Terrence J. Sejnowski

## Abstract

The Independent Component Analysis (ICA) algorithm<sup>1</sup> is a new information-theoretic approach to the problem of separating multichannel electroencephalographic (EEG) data into independent sources<sup>2</sup>. We tested the potential usefulness of the ICA algorithm for EEG source decomposition by applying the algorithm to simulated EEG data. These data were synthesized by projecting 6 known input signals from single- and multiple-dipole sources in a three-shell spherical model head<sup>3</sup> to 6 simulated scalp sensors.

In different simulations, we (1) altered the relative source strengths, (2) added multiple low-level sources (weak brain sources and sensor noise) to the simulated EEG, and (3) permuted the simulated dipole source locations and orientations. The algorithm successfully and reliably separated the activities of relatively strong sources from the activities of weaker brain sources and sensor noise, regardless of source locations and dipole orientations. These results suggest that the ICA algorithm should be able to separate temporally independent but spatially overlapping EEG activities arising from relatively strong brain and/or non-brain sources, regardless of their spatial distributions.

# 1 Introduction

Multichannel electromagnetic recordings from the scalp, including EEG, magnetoencephalographic (MEG), event-related potential (ERP) and event-related field (ERF) data, have been widely used to study dynamic brain processes involved in perception, memory, selective attention, recognition, and priming. However, the underlying brain processes which produce fields recorded at the scalp are largely undetermined. The most common model for EEG generation assumes that electrodes placed on the scalp surface record the electromagnetic activity of local or distributed cortical neural networks which form effective single- or multiple-dipole sources (Fig 1a)<sup>4, 5, 6</sup>.

EEG recordings consist of a complex distribution of overlapping source activities, making it difficult to identify the contributing independent sources. The problem of separating sources without *a priori* knowledge of their number or spatial distribution is known as “blind separation”. Most existing techniques for approaching the problem of source separation employ second-order statistical methods (e.g. covariance, cross-correlation, and principle component analysis).<sup>6</sup> The Independent Component Analysis (ICA) algorithm<sup>1</sup> we use is a blind separation technique based on information-maximization which uses higher-order statistical information. The algorithm has been recently shown to produce useful decompositions of EEG data<sup>2</sup>, separating identifiable EEG components (e.g., alpha waves and steady-state responses<sup>7, 8</sup>) into individual output channels.

However, without prior knowledge of the actual brain sources which contribute to the EEG, it is difficult to verify the algorithm’s effectiveness. We assume there

may be a few strong sources active during a given EEG recording period along with a larger number of relatively weak sources. In addition, low-level sensor noise may contaminate scalp recordings. To determine whether the ICA algorithm can successfully separate relatively strong signals mixed with numerous weaker signals, we performed several simulation experiments.

We simulated the activities of 6 brain source signals projected in a three-shell spherical head model<sup>3</sup> by volume conduction to 6 scalp electrodes and applied the ICA algorithm to resulting simulated EEG signals. The simulations allowed us to investigate changes in ICA algorithm performance with variations in source strength, location, and orientation as well as effects of adding simulated weak brain signals and sensor noise to the simulated EEG.

## 1.1 The ICA algorithm

The algorithm is based on an ‘infomax’ neural network<sup>1, 9, 10</sup>. It finds, by stochastic gradient ascent, a matrix,  $\mathbf{W}$ , which maximizes the entropy,<sup>11</sup>  $H(\mathbf{y})$ , of an ensemble of ‘sphered’ input vectors  $\{\mathbf{x}_s(t)\}$ , linearly transformed and sigmoidally compressed:

$$\mathbf{u}(t) = \mathbf{W}\mathbf{x}_s(t), \mathbf{y} = g(\mathbf{u}(t)) \quad (1)$$

The ‘unmixing’ matrix  $\mathbf{W}$  performs source separation, while the sigmoidal nonlinearity  $g()$  provides necessary higher-order statistical information. Initial sphering of the zero-mean input data<sup>12</sup>:

$$\mathbf{x}_s(t) = \mathbf{P}\mathbf{x}(t) \quad (2)$$

where  $\mathbf{P}$  is twice the matrix square root of the inverse of the covariance matrix, used to speed convergence:

$$\mathbf{P} = 2\langle\mathbf{x}\mathbf{x}^T\rangle^{-\frac{1}{2}} \quad (3)$$

$\mathbf{W}$  is then initialized (in our simulations with random values between 0.1 and 1.0), and iteratively adjusted using small batches of data vectors drawn randomly from  $\{\mathbf{x}_s(t)\}$  without substitution, according to:

$$\Delta \mathbf{W} = \epsilon \frac{\partial H(\mathbf{y})}{\partial \mathbf{W}} \mathbf{W}^T \mathbf{W} = \epsilon (\mathbf{I} + \hat{\mathbf{y}} \mathbf{u}^T) \mathbf{W}, \quad (4)$$

where  $\epsilon$  is the learning rate,  $\mathbf{I}$  is the identity matrix, and vector  $\hat{\mathbf{y}}$  has elements

$$\hat{y}_i = (\partial / \partial u_i) \ln(\partial y_i / \partial u_i) \quad (5)$$

The  $(\mathbf{W}^T \mathbf{W})$  ‘natural gradient’ term in the update equation<sup>13</sup> avoids matrix inversions and speeds convergence. We use the logistic nonlinearity,  $g(u_i) = (1 + \exp(-u_i))^{-1}$ , for which  $\hat{y}_i = 1 - 2y_i$ . When ICA algorithm is trained on EEG data, the rows of the resultant matrix  $(\mathbf{W}\mathbf{P})$  are linear spatial filters which, applied to the input data, produce source activity waveforms  $(\mathbf{W}\mathbf{P}\mathbf{x}(t))$ . The columns of the inverse weight matrix  $(\mathbf{W}\mathbf{P})^{-1}$  represent the projection weights from the ICA algorithm sources to the sensor array. Further details and references about the algorithm appear in 1, 13, 14, 15, other related approaches and background material in 10, 16, 17, 18, 19.

## 2 Methods

An overview of the simulation process is given in Fig. 2.

### 2.1 The three-shell spherical head model

In our simulations, we used a three-shell spherical head model which projects dipoles at 4 fixed brain locations onto 6 scalp electrodes. The projection matrix containing the model parameters was precomputed by Anders Dale using an analytic representation for a three-shell spherical head model<sup>3, 20</sup>. Electrode positions were vertices of a

triangulated icosahedron located on the model head sphere. At each of the 4 locations in the head model, we placed 1 to 3 dipoles pointing in different directions, giving a total of 7 dipoles. We assigned 5 input signals to single dipoles, and 1 input signal (Fig. 2a) to two bilateral dipoles (Fig. 2b). As shown in Fig. 2, two dipoles with different orientations were placed at a single dipole location, and three dipoles with different orientations were placed at another location.

These choices were expressed via a  $((4 \times 3) \times 6)$  configuration matrix,  $\mathbf{C}$ , which assigned 6 source signals to the 7 dipoles according to the configuration described above. The configuration matrix was then multiplied by the  $(6 \times (4 \times 3))$  weight matrix,  $\mathbf{F}$ , which projected the 7 dipoles (at the 4 dipole locations) to each of the 6 selected electrode sites. The resulting matrix product:

$$\mathbf{M} = \mathbf{FC} \tag{6}$$

was a  $6 \times 6$  “mixing” matrix specifying the simulated EEG signals as linear combinations of the 6 input sources. Simulation variables were chosen such that this mixing matrix was non-singular. Note that despite the complexity of the head model, the mixing matrix was a linear  $6 \times 6$  transformation of the 6 sources, and therefore satisfied the assumptions of the ICA algorithm.

## 2.2 Input signals

The input signals were six 7.5-sec (79,119-point) segments of acoustic signals consisting of speech signals (“iris” and “zach”), drum tapping sounds (“drum”), a sounding gong (“gong”), a choral excerpt from Handel’s Messiah (“handel”), and a keyboard synthesizer sequence (“synth”). Each signal was recorded by the auxiliary microphone of a Sparc-10 workstation<sup>1</sup>. Before the simulations, each input was made zero-mean

and normalized by linear scaling to fit within the  $[-1, 1]$  interval.

### **2.3 Source strength adjustment**

To simulate sources with varied strengths, the vector of input signals,  $\mathbf{s}(t)$ , were scaled relative to one another in steps of -8 dB (Fig. 3) using a  $6 \times 6$  diagonal attenuation matrix,  $\mathbf{A}$ . Simulated EEG signals,  $\mathbf{x}(t)$ , were derived from the input signals by multiplying by the attenuation and mixing matrices.

$$\mathbf{x}(t) = \mathbf{M}\mathbf{A}\mathbf{s}(t) \quad (7)$$

### **2.4 Weak brain sources**

In some experiments, seven simulated weak brain source signals were added to the simulated EEG. These (“brain noise”) sources consisted of uncorrelated random noise with a flat distribution in the  $[-1,1]$  interval, scaled to -40 dB below the strongest input signal (i.e., at the same level as the weakest input signal) (Fig. 3). The 7 brain noise sources were assigned to simulated “diffuse” dipoles placed close to each of the 7 brain source dipoles by adding 1% gaussian-distributed noise to the matrix,  $\mathbf{M}$ , before mixing. The mixed brain noise signals were then added to the simulated EEG.

### **2.5 Sensor noise**

To simulate EEG sensor noise, uniformly-distributed white noise was added to each sensor signal at an intensity of -64 dB below the mean level of the simulated EEG signals. These noise sources were uncorrelated with each other.

## 2.6 ICA algorithm training

Training with the ICA algorithm began with an initial learning rate of 0.004. This was reduced to 0.0015 after the first training step. Thereafter, a heuristic method was used to reduce or increase the learning rate at each time step according to the net change in weights from the previous step. This change was computed by taking the sum of squares of the changes in weights between the current and previous time steps. Whenever the net weight change was less than  $10^{-7}$ , the learning rate was multiplied by 5/8ths. If the learning rate went below  $10^{-7}$ , it was increased to  $4 \times 10^{-6}$  and the input data was reshuffled to avoid overlearning. Training was stopped after 32 steps. All computations were performed using Matlab (version 4.2c) on a Sun 670MP with 64 megabytes of RAM and a 40MHz processor (equivalent to a Sparc 2).

## 2.7 Performance measures

### 2.7.1 SNR in the ICA algorithm output

Our measure of the ICA algorithm's performance was the signal-to-noise ratio (SNR) of each input signal in the output sources. For each input signal,  $s_i(t)$ , we defined:

$$\mathbf{s}_i(t) = \begin{pmatrix} 0 \\ \vdots \\ 0 \\ s_i(t) \\ 0 \\ \vdots \\ 0 \end{pmatrix} \quad (8)$$

in which all input signals except for  $s_i(t)$  were zeroed out. The output source waveforms for  $\mathbf{s}_i(t)$  were then defined as:

$$\mathbf{u}_i(t) = \mathbf{WPMAs}_i(t) \quad (9)$$

The *signal level*,  $S_{ik}^{ICA}$ , of the  $i$ th input signal in the  $k$ th output source waveform was computed by taking the standard deviation of the  $k$ th row of  $\mathbf{u}_i(t)$ . The noise level for each input signal in each output source was computed by letting  $\mathbf{s}_i^c(t)$  consist of all input signals *except*  $s_i(t)$ :

$$\mathbf{s}_i^c(t) = \begin{pmatrix} s_1(t) \\ \vdots \\ s_{i-1}(t) \\ 0 \\ s_{i+1}(t) \\ \vdots \\ s_n(t) \end{pmatrix} \quad (10)$$

These “complementary” signal vectors were passed through the simulated mixing and unmixing processes with brain noise and sensor noise sources added, giving output source waveforms:

$$\mathbf{u}_i^c(t) = \mathbf{WP}\{\mathbf{MA}[\mathbf{s}_i^c(t) + \mathbf{n}(t)] + \mathbf{r}(t)\} \quad (11)$$

where  $\mathbf{n}(t)$  is the weak brain sources and  $\mathbf{r}(t)$  is the sensor noise. The *noise level*,  $N_{ik}^{ICA}$ , was defined as the standard deviation of the  $k$ th row of  $\mathbf{u}_i^c(t)$ . Then, the SNR of the  $i$ th signal in the ICA algorithm source waveforms was defined as:

$$SNR_i^{ICA} = \max_{k=1, \dots, n} (20 \log_{10}(\frac{S_{ik}^{ICA}}{N_{ik}^{ICA}})) \quad (12)$$

where  $n$  is the number of sources.

### 2.7.2 SNR in the simulated EEG

The SNR of each input signal in the simulated EEG was computed for comparison with the SNR in the ICA output. The signal level,  $S_{ij}^{EEG}$ , for the  $i$ th input signal

in the simulated EEG signal was defined as the standard deviation of the simulated EEG in the  $j$ th recording electrode (i.e. in the  $j$ th row of  $\mathbf{x}_i(t)$ ):

$$\mathbf{x}_i(t) = \mathbf{M}\mathbf{A}\mathbf{s}_i(t) \quad (13)$$

The noise level,  $N_{ij}^{EEG}$ , for the  $i$ th input signal was defined as the standard deviation of the  $j$ th row of the complementary mixed signal matrix:

$$\mathbf{x}_i^c(t) = \mathbf{M}\mathbf{A}[\mathbf{s}_i^c(t) + \mathbf{n}(t)] + \mathbf{r}(t) \quad (14)$$

SNR of the  $i$ th input signal in the simulated EEG was then defined as:

$$SNR_i^{EEG} = \max_{j=1,\dots,m} (20\log_{10}(\frac{S_{ij}^{EEG}}{N_{ij}^{EEG}})) \quad (15)$$

where  $m$  is the number of sensors.

### 2.7.3 SNR gain from EEG to ICA algorithm outputs

For each input signal, the difference between its  $SNR^{ICA}$  and  $SNR^{EEG}$  was defined as the SNR gain,  $G$ , resulting from ICA algorithm source separation.

$$G_i = SNR_i^{ICA} - SNR_i^{EEG} \quad (16)$$

## 2.8 Four simulation experiments

We conducted four simulation experiments to test the efficacy and reliability of the ICA algorithm in performing blind separation of EEG signals. Each experiment consisted of six different ICA algorithm trainings:

**Experiment 1: Without noise sources.** To study the effect of different initial weights,  $\mathbf{W}$ , and data presentation orders on the output of the ICA algorithm,

we trained the algorithm with randomized initial weight matrices and input data presentation orders.

**Experiment 2: With noise sources.** The simulations above were repeated with the 13 noise sources (7 weak brain sources and 6 sensor noise sources) added to the simulated EEG signals to test the source separation performance of the algorithm under realistic conditions.

**Experiment 3: Varying input signal strength assignments.** Performance of the ICA algorithm may depend in part on the statistical distributions of the input signals<sup>12</sup>. To test whether differences in the input signal distributions were responsible for the results of Experiment 2, we circularly permuted the order of assignment of input signals (by rotating the rows of  $\mathbf{s}(t)$ ) to attenuation levels  $\mathbf{A}$  (eqn. 7).

**Experiment 4: Varying input signal source assignments.** In previous experiments, the assignment of stronger and weaker signals to model brain sources was fixed. In this experiment, we varied the attenuated signal assignments to brain sources across ICA algorithm trainings. First, we attenuated the input signals in the same order as in Experiment 1. We then circularly permuted the assignment of the attenuated input signals to brain sources (by rotating the rows of  $\mathbf{As}(t)$  before multiplying by  $\mathbf{M}$  in equation 7).

## 3 Results

### 3.1 ICA algorithm performance without low-level sources

With simulated weak brain sources and sensor noise sources turned off, the ICA algorithm consistently separated each source into a different output channel regardless of differences in signal amplitudes (Fig. 4) and the algorithm's initial conditions. The results confirmed similar findings reported for earlier audio simulations<sup>1</sup>. Each input signal was separated into a different output channel with an  $SNR^{ICA}$  of at least 30 dB. The SNR gain,  $G$ , for the 6 input signals ranged from 21 dB to 67 dB. Although both the input signal levels and  $SNR^{ICA}$  varied widely between signals (ranges of 40 dB and 36 dB respectively), each input source was separated cleanly into a separate ICA algorithm output channel. This result was highly reproducible; standard deviations of  $SNR^{ICA}$  across trainings were all less than 1 dB. Most SNR gain occurred during the first training step.

### 3.2 Effects of adding low-level sources

When the 13 low-level sources were added to the simulated EEG, separation remained strong for the two strongest input sources ( $SNR^{ICA} > 20$  dB) (Fig. 5), moderate for the two next-strongest signals ( $SNR^{ICA} > 8$  dB), and weak for the weakest two input signals ( $SNR^{ICA} < -10$  dB). SNR gains for the 6 brain sources ranged from 12 dB to 29 dB. Nearly all SNR gain occurred during the first 5 training steps.

### 3.3 Effects of varying input signal strength assignments

Mean differences in  $SNR^{ICA}$  for the 6 input signals closely followed their relative input amplitudes (Fig. 6). The range of mean  $SNR^{ICA}$  values (39 dB) was again

close to the range of input levels (40 dB). The SNR gain for the 6 input signals ranged from 13 dB to 31 dB. Stronger sources appeared in individual ICA output channels while weaker ones (and noise sources) were mixed in remaining channels.

### **3.4 Effects of varying source assignments**

For each permutation of signal-to-source assignments, the ICA algorithm gave results comparable to those in Experiment 3. The range of mean  $SNR^{ICA}$  (39 dB) closely matched the range of input signal strengths (40 dB) (Fig. 7). SNR gains ranged from 14 dB to 30 dB.

## **4 Conclusion**

The reported effectiveness of the ICA algorithm in separating multiple linearly-mixed sources<sup>1, 9, 10</sup> was reproduced in our EEG simulations using a three-shell head model with 6 input signals. Previously, performance of the algorithm in the presence of multiple weak brain sources and noise sources had not been systematically investigated. In our experiments, relatively strong simulated EEG signals were successfully and repeatedly separated with SNR gains averaging 22 dB. Our results indicate that the performance of the algorithm degrades gracefully in the presence of multiple weak independent sources.

## **5 Discussion**

The Independent Component Analysis algorithm appears to be a promising tool for the analysis of highly correlated multichannel EEG signals. Our results suggest that relatively strong brain EEG sources may be effectively separated from weak brain and

noise signals with SNR gains of 20 dB and above. Applications of ICA algorithm to averaged event-related potentials (ERPs) may be particularly promising since response averaging increases the amplitudes of activity, time- and phase-locked to experimental events, relative to the activities of all other spontaneous (i.e. non-phase locked) EEG sources. The number of independent strong brain sources contributing to ERP data may be smaller than the number of EEG channels typically used to record them<sup>15</sup>. In that case, most or all of the ERP sources may be separable using the ICA algorithm. This algorithm could be used to compare the time courses and relative strengths of ERP source activations in different experimental conditions. Since the algorithm describes *what* independent sources produce its input data, not *where* these sources are spatially located, neurophysiological interpretation of the ICA algorithm sources poses a further research challenge.

## **Acknowledgements**

This report was supported in part by grants to S.M., T-P.J. and T.J.S. from the Office of Naval Research, and to T.J.S. from the Howard Hughes Medical Institute. The authors wish to thank Anders Dale for supplying the head model parameters.

## References

1. Bell, A.J. & Sejnowski, T.J. An information-maximization approach to blind separation and blind deconvolution, *Neural Computation* **7**, 1129-1159 (1995).
2. Makeig, S., Bell, A.J., Jung, T-P. & Sejnowski T.J. Independent component analysis of electroencephalographic data. *Advances in Neural Information Processing Systems* **8**, MIT Press (1996).
3. Dale, A.M. & Sereno, M.I. Improved localization of cortical activity by combining EEG and MEG with MRI cortical surface reconstruction - a linear approach. *J. Cogn. Neurosci.* **5**, 162-176 (1993).
4. Nunez, P.L. *Electric Fields of the Brain* . New York: Oxford (1981).
5. Scherg, M. & Von Cramon, D. Evoked dipole source potentials of the human auditory cortex. *Electroencephalogr. Clin. Neurophysiol.*, **65** , 344-60 (1986).
6. Chapman, R.M. & McCrary, J.W. EP component identification and measurement by principal components analysis. *Brain and Language* **27**, 288-301 (1995).
7. Pantev, C., Elbert, T., Makeig, S., Hampson, S., Eulitz, C. & Hoke, M. Relationship of transient and steady-state auditory evoked fields. *Electroencephalogr. Clin. Neurophysiol.* **88**, 389-396 (1993).
8. Galambos, R., Makeig, S. & Talmachoff P. A 40 Hz auditory potential recorded from the human scalp, *Proc. Natl. Acad. Sci. USA* **78**, 2643-2647 (1981).
9. Linsker, R. Local synaptic learning rules suffice to maximise mutual information in a linear network. *Neural Computation* **4**, 691-702 (1992).

10. Nadal, J-P. & Parga, N. Non-linear neurons in the low noise limit: a factorial code maximises information transfer. *Network* **5**, 565-581 (1994).
11. Cover, T.M. & Thomas, J.A. *Elements of Information Theory*, John Wiley (1991).
12. Bell, A.J. & Sejnowski, T.J. Learning the higher-order structure of a natural sound, *Network: Computation in Neural Systems* **7**, 2 (1996).
13. Amari S., Cichocki, A. & Yang, H.H. A new learning algorithm for blind signal separation. In *Advances in Neural Information Processing Systems* 8, MIT Press (1996).
14. Bell, A.J. & Sejnowski, T.J. Fast blind separation based on information theory. *Proc. Intern. Symp. on Nonlinear Theory and Applications*, Las Vegas (1995).
15. Makeig, S., Jung T-P., Bell, A.J., Ghahremani, D., and Sejnowski, T. S. Blind separation of event-related brain responses into independent components. *Nature*. (submitted)
16. Cardoso, J-F. & Laheld, B. Equivalent adaptive source separation, *IEEE Trans. Signal Proc.* (to appear).
17. Comon, P. Independent component analysis, a new concept? *Signal Processing* **36**, 287-314 (1994).
18. Jutten, C. & Herault, J. Blind separation of sources, part I: an adaptive algorithm based on neuromimetic architecture. *Signal Processing* **24**, 1-10 (1991).

19. Karhunen, J., Oja, E., Wang, L., Vigario, R. & Joutsenalo, J. A class of neural networks for independent component analysis, *IEEE Trans. Neural Networks* (to appear).
20. Kavanagh R.N., Darcey T.M., Lehmann D., and Fender D.H. Evaluation of methods for three-dimensional localization of electrical sources in the human brain. *IEEE Trans. Biomed. Eng.* **9** , 25:421-429 (1978).

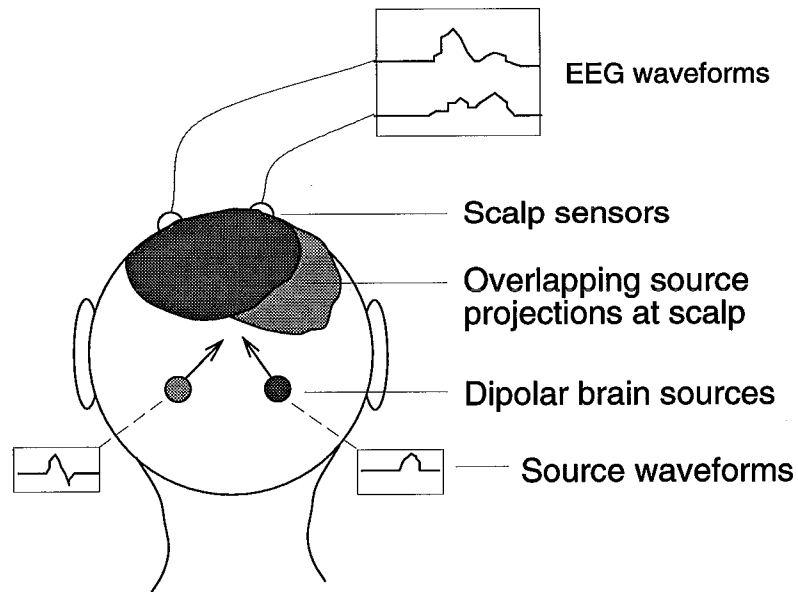


Figure 1: **Schematic illustration of two dipole sources with overlapping projections to the scalp.** Activities of each dipole (*“source waveforms”*) are projected to the scalp through three conductive layers (brain, skull, and scalp). The scalp sensors record potentials (*“EEG waveforms”*) which sum activity from both dipoles.

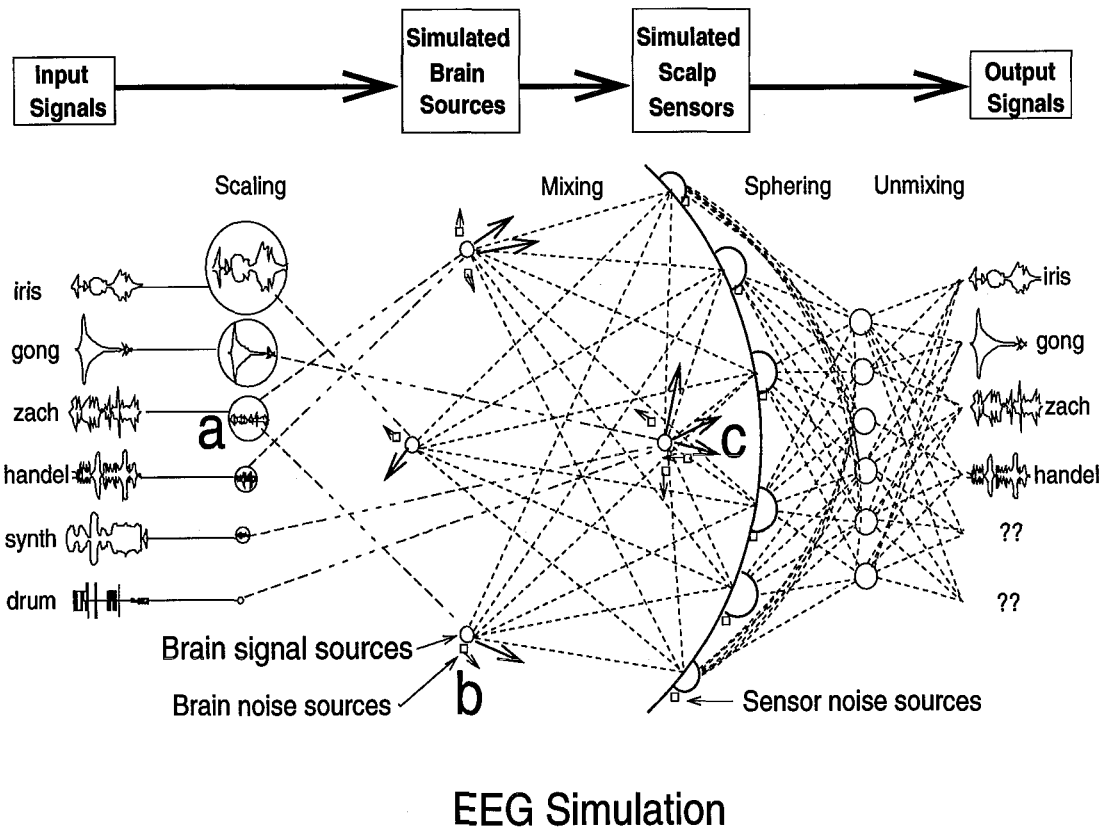


Figure 2: **Schematic overview of the simulations.** Input signals were scaled relative to one another (*circles under “Scaling”*) and assigned to single- or multiple-dipole brain sources (*long arrows*). One signal (*a*) (*here, “zach”*) was assigned to a bilateral dipole source (*b*) simulating, for example, a bitemporal source in the auditory cortices. Other signals (*here, for instance, “gong”, “synth”, and “drum”*) were assigned to sources modeled as single dipoles with different orientations at the same brain location (*c*). Seven weak brain (or “brain noise”) sources (*small arrows*) were positioned near the seven signal dipoles. The 6 input signal sources and 7 brain noise signals were mixed at the 6 simulated EEG sensors on the scalp surface (*semicircles*). Uncorrelated low-level “sensor noise” signals (*small boxes near sensors*) was added to the simulated EEG at each of the scalp sensors. After an initial “sphering” of the simulated EEG data, source separation was performed via the “unmixing” matrix produced by the ICA algorithm. Spatial filtering of the simulated EEG with the sphering and unmixing matrices produced output source signals. Four of these (*labeled “iris”, “gong”, “zach”, and “handel”*) were highly correlated with their respective input signals. Two other ICA algorithm outputs (*labeled “??”*) mixed the remaining two weakest input signals (“*synth*” and “*drum*”) with the noise signals. (See <http://www.cnl.salk.edu/~dara/icasim> for an audio presentation of the signals at each stage of the simulation).

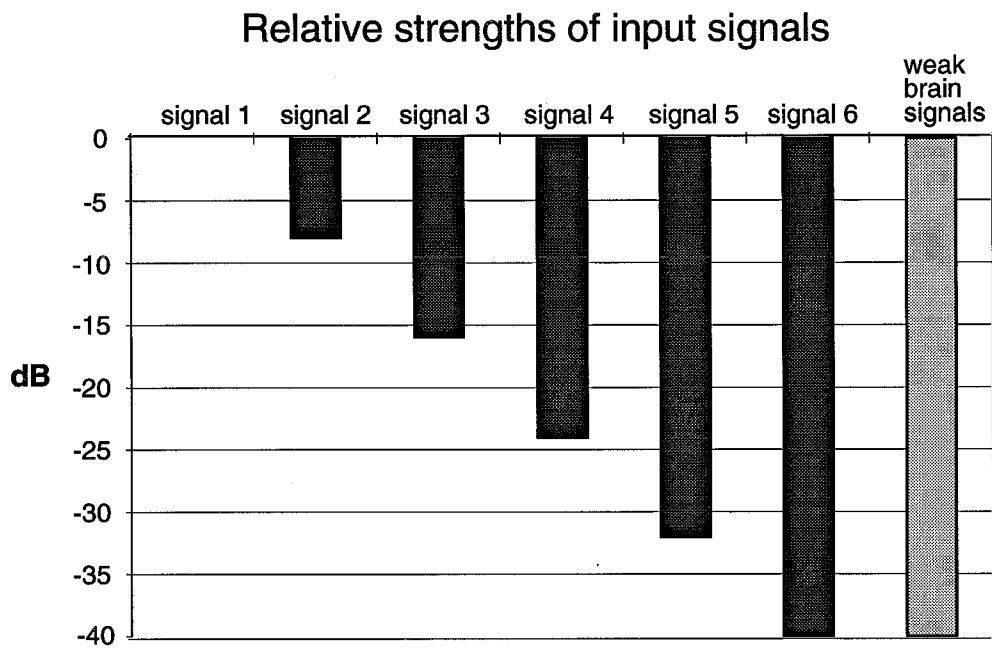


Figure 3: **Relative strengths of input signals.** Input signals were scaled relative to one another in -8 dB steps. The 7 weak brain (or “brain noise”) sources added to the simulated EEG in Experiments 2-4 (*rightmost bar*) were scaled to the level of the weakest input signal.

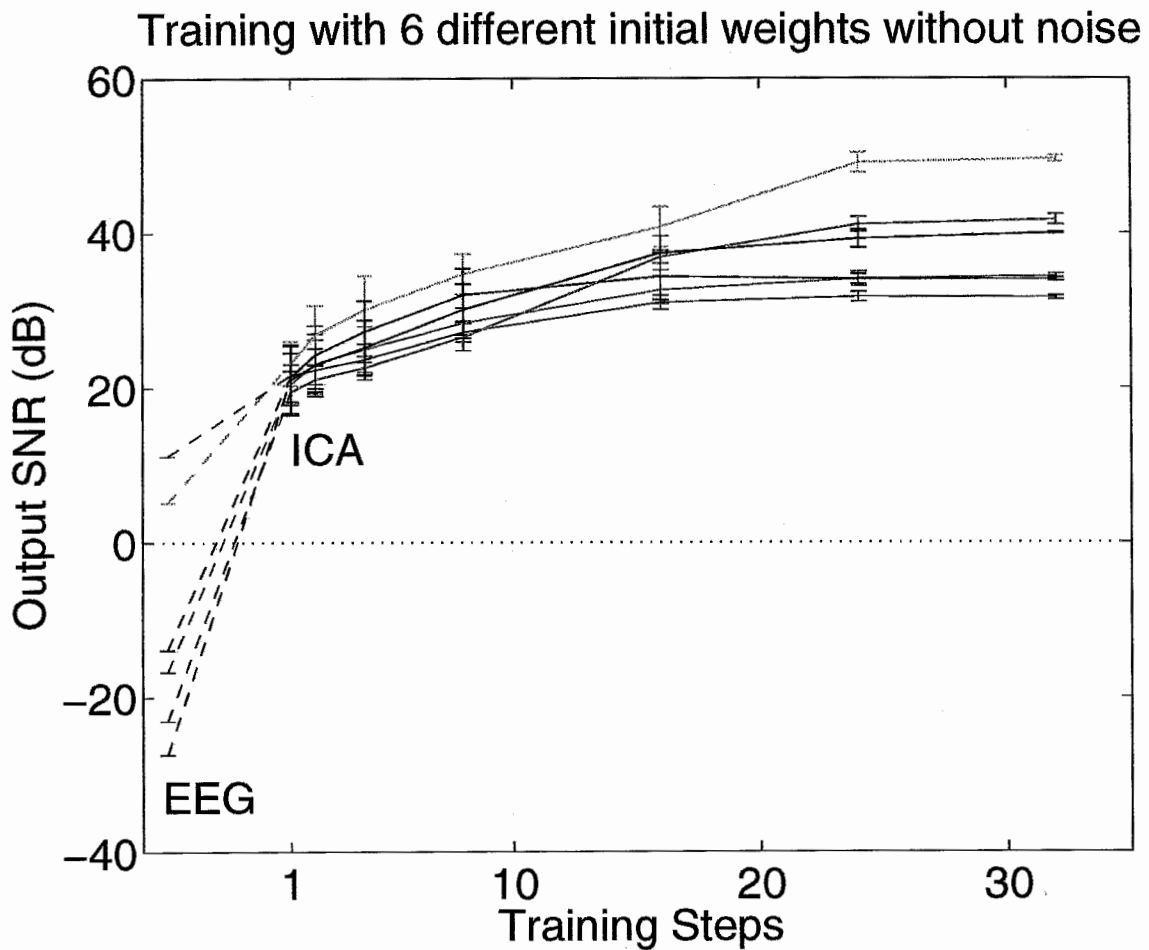


Figure 4: **Experiment 1.** Output signal-to-noise ratio (SNR) for each input signal in the simulated EEG signals (*dashed lines*) and during ICA algorithm training. ICA algorithm separation performance was strong and consistent across all sources and multiple training runs.

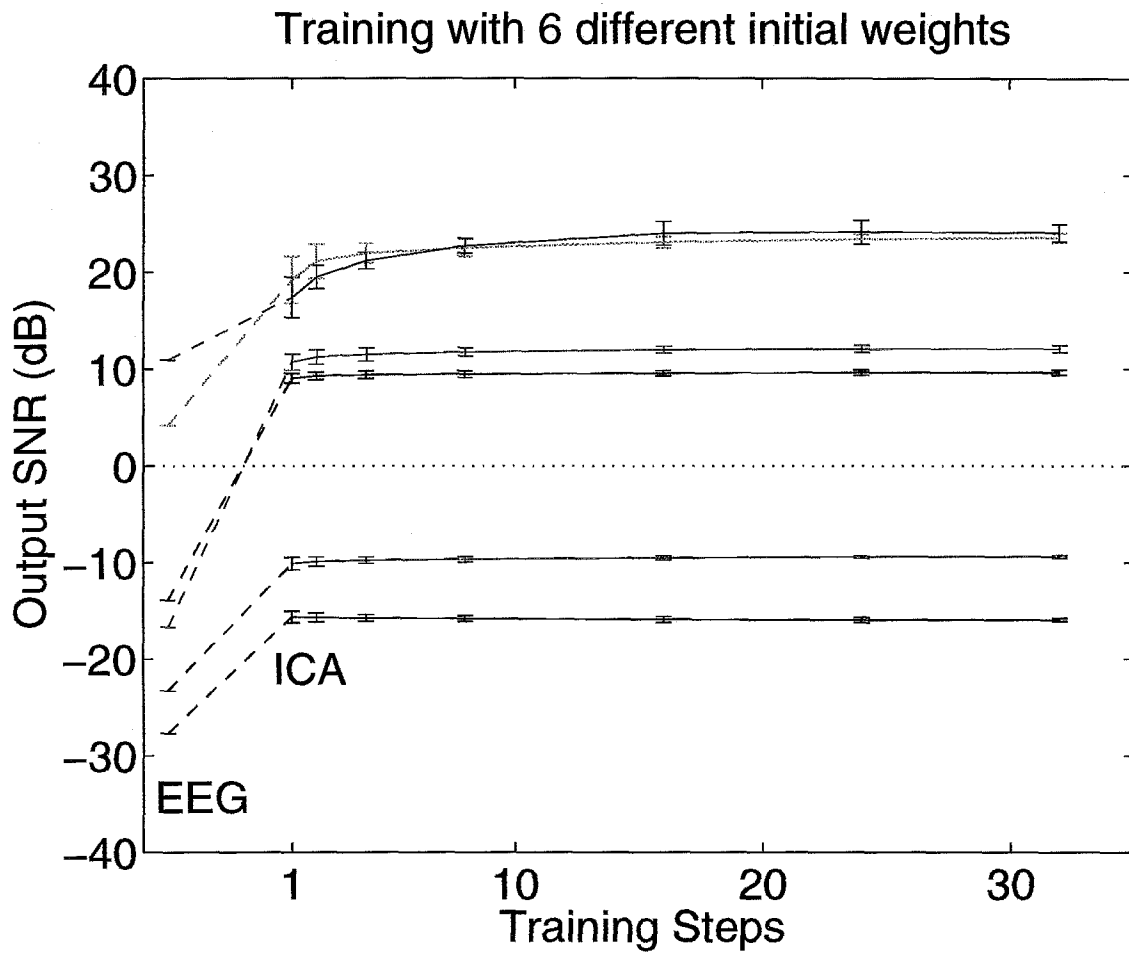


Figure 5: **Experiment 2.** When 13 additional low-level sources (7 weak brain sources, 6 sensor noise sources) were added to the simulated EEG, ICA performance in separating the 6 input signals was favorable ( $> 20$  dB) for strongest input signals, and poor ( $< -10$  dB) for relatively weak inputs. SNR gains (*difference between EEG and final ICA SNR values*) ranged from 12 dB to 29 dB for the six signals.

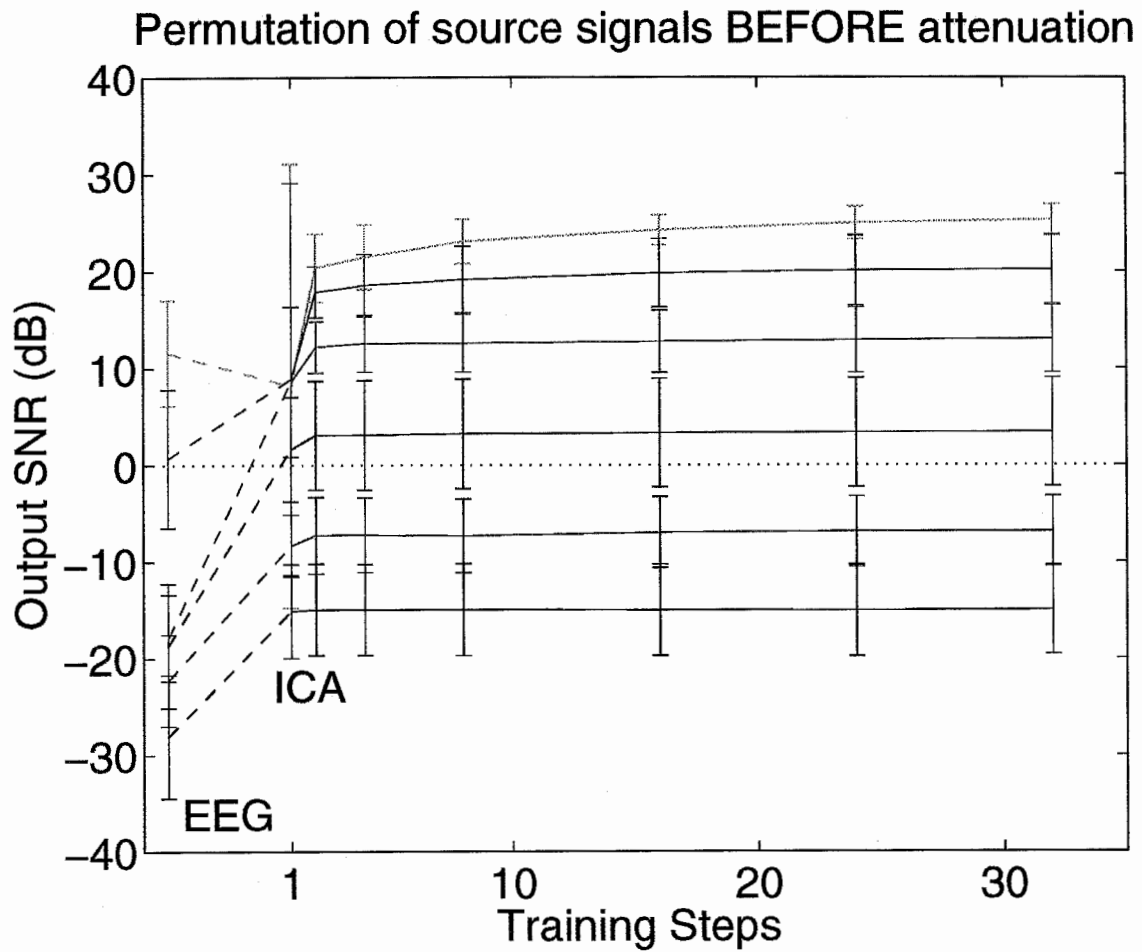


Figure 6: **Experiment 3.** Blind separation performance by the ICA algorithm for 6 permutations of input signal ordering prior to attenuation (*see Section 2.8 of text*). The order of signal attenuation was reproduced in the output SNR. The range of output SNR values after 32 training steps (*rightmost values*) was close to the 40 dB range of relative input signal strengths. SNR gains for the 6 sources ranged from 13 dB to 31 dB.

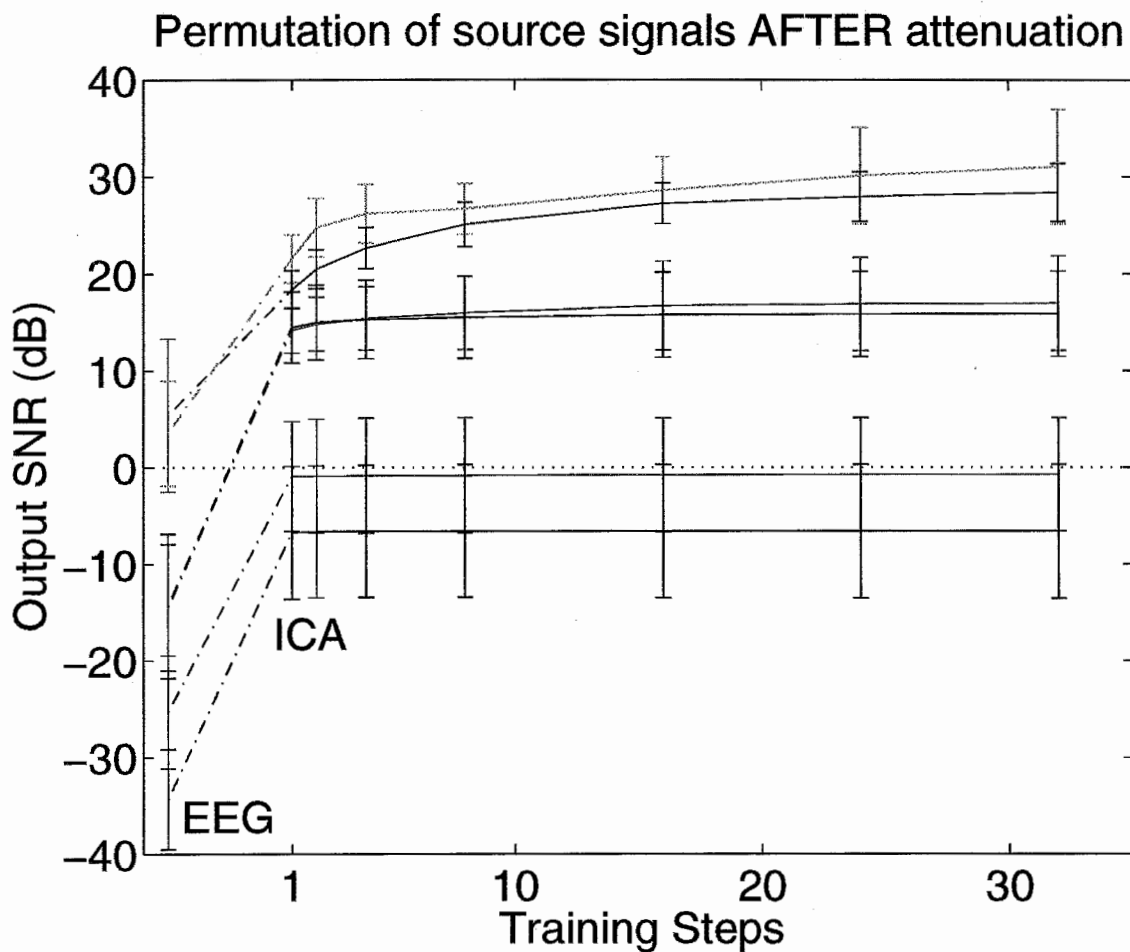


Figure 7: **Experiment 4.** ICA algorithm performance for six different orders of assignments of attenuated input signals to brain sources (*see Section 2.8 of text*). Again, stronger signals were separated better than weaker signals, and the range of mean output SNRs (39 dB) was nearly equal to the input signal scaling range (40 dB). SNR gains for the 6 sources ranged from 14 dB to 30 dB.